The Astrophysical Journal, 694:1010–1018, 2009 April 1 doi:10.1088/0004-637X/694/2/1010

LOCALITY OF MHD TURBULENCE IN ISOTHERMAL DISKS

Xiaoyue Guan[1], Charles F. Gammie[1,2], Jacob B. Simon[3], and Bryan M. Johnson[4]
[1] Astronomy Department, University of Illinois, 1002 West Green Street, Urbana, IL 61801, USA
[2] Physics Department, University of Illinois, 1100 West Green Street, Urbana, IL 61801, USA
[3] Astronomy Department, University of Virginia, Box 400325, Charlottesville, VA 22904, USA
[4] Lawrence Livermore National Laboratory, L-023, 7000 East Avenue, Livermore, CA 94550, USA
Received 2008 October 6; accepted 2009 January 6; published 2009 March 20

ABSTRACT

We numerically evolve turbulence driven by the magnetorotational instability (MRI) in a three-dimensional, unstratified shearing box and study its structure using two-point correlation functions. We confirm Fromang and Papaloizou's result that shearing box models with zero net magnetic flux are not converged; the dimensionless shear stress α is proportional to the grid scale. We find that the two-point correlation of $\boldsymbol{B}$ shows that it is composed of narrow filaments that are swept back by differential rotation into a trailing spiral. The correlation lengths along each of the correlation function principal axes decrease monotonically with the grid scale. For mean azimuthal field models, which we argue are more relevant to astrophysical disks than the zero net field models, we find that: α increases weakly with increasing resolution at fixed box size; α increases slightly as the box size is increased; α increases linearly with net field strength, confirming earlier results; the two-point correlation function of the magnetic field is resolved and converged, and is composed of narrow filaments swept back by the shear; the major axis of the two-point increases slightly as the box size is increased; these results are code independent, based on a comparison of `ATHENA` and `ZEUS` runs. The velocity, density, and magnetic fields decorrelate over scales larger than $\sim H$, as do the dynamical terms in the magnetic energy evolution equations. We conclude that MHD turbulence in disks is localized, subject to the limitations imposed by the absence of vertical stratification, the use of an isothermal equation of state, finite box size, finite run time, and finite resolution.

Key words: accretion, accretion disks – MHD

1. INTRODUCTION

Astrophysical disks appear to redistribute angular momentum rapidly, much more rapidly than one would expect based on estimates of the molecular viscosity. Classical thin accretion disk theories (Shakura & Sunyaev 1973; Lynden-Bell & Pringle 1974) solved this problem by appealing to turbulence, and modeled the effects of this turbulence as an "anomalous viscosity." The idea that turbulence plays a key role was placed on firmer foundations with the (re)discovery of the magnetorotational instability (MRI; Balbus & Hawley 1991) and subsequent numerical investigations (see Balbus & Hawley 1998 for a review). Winds or gravitational instability may drive disk evolution in certain cases, but MRI-initiated MHD turbulence appears capable of driving disk evolution in a wide variety of astrophysical disks.

We still do not know, however, whether the effects of MHD turbulence on disks are localized. It is possible that structures develop that are large compared to a scale height $H \equiv c_s/\Omega$, and that these structures are associated with nonlocal energy and angular momentum transport. If so, disk evolution would not be well described by a theory, such as the α model, in which the shear stress depends only on the local surface density and temperature.

A related possibility, which we will not examine here, is that the time-averaged turbulent stresses $\overline{W}_{r\phi}$ might satisfy $\partial \overline{W}_{r\phi}/\partial \Sigma < 0$ ($\Sigma \equiv$ surface density; see Piran 1978 for a discussion). That is, the disk might be "viscously" unstable. This could cause the disk to break up into rings or even—to use a term of art—"blobs." Such an outcome would be awkward for the classic phenomenological steady disk and disk evolution models, which have had some success in modeling cataclysmic variable disks and black hole X-ray binary disks in a high, soft state (e.g., Belloni et al. 1997; Lasota 2001).

How can one probe the locality of MHD turbulence in disks? We will use the two-point correlation function of the magnetic field, velocity field, and density as determined by numerical experiments. Nonlocal transport would likely be associated with features in the two-point correlation function, as would viscous instabilities. For example, turbulence might excite waves (wakes) that carry energy and angular momentum over many H in radius before damping. These wakes would appear as extended features in the two-point correlation function.

The two-point correlation function and the power spectrum contain the same information since they are related by a Fourier transform. But they do not convey the same impression and they have different noise properties. For a one-dimensional function sampled at N points over an interval L half the sample points in the power spectrum lie between the Nyquist frequency ($\pi N/L$) and half the Nyquist frequency, while for the correlation function half the sample points lie between a separation $L/4$ and $L/2$. The two-point correlation function will therefore convey a more accurate impression of large-scale features than power spectra.

In this paper, we study models with both zero net field and net azimuthal field. We ignore mean vertical field models because we remain persuaded by the phenomenological argument of van Ballegooijen (1989) that vertical field diffuses easily out of the disk when the turbulent magnetic Prandtl number is $O(1)$ (although there are ways of evading this argument; Spruit & Uzdensky 2005). Net azimuthal field models are, we think, most relevant to astrophysical disks. In disk galaxies—the only differentially rotating disks where we can resolve field structure—the azimuthal field dominates when averaged over areas more than a few H^2 in extent (e.g., Beck 2007). Azimuthal

field also dominates in global disk simulations (e.g., Hirose et al. 2004; McKinney & Narayan 2007; Beckwith et al. 2008), and in local disk simulations. In local simulations in which the mean field is allowed to evolve (e.g., Brandenburg et al. 1995; Miller & Stone 2000) an azimuthal mean field develops. Taken together these simulations and observations strongly suggest that the azimuthal field averaged over regions $\sim H^2$ in area will never be exactly zero.

This paper is organized as follows. In Section 2, we give a simple description of the local model and summarize our numerical algorithm with orbital advection. We then study zero net flux models (as in Fromang & Papaloizou 2007; hereafter FP07); this serves as a code test and introduces the correlation function analysis. In Section 3, we explore the properties of turbulence in models with a mean azimuthal field. We report on the saturation level and correlation lengths and we discuss their dependence on the model parameters, such as resolution, box size, and initial field strength. Section 4 contains a summary and guide to our results.

2. MODEL, METHODS, AND TESTS

Our starting point is the local model for disks. It is obtained by expanding the equations of motion around a circular-orbiting coordinate origin at cylindrical coordinates $(r, \phi, z) = (r_o, \Omega_o t + \phi_o, 0)$, assuming that the peculiar velocities are comparable to the sound speed and that the sound speed is small compared to the orbital speed. The local Cartesian coordinates are obtained from cylindrical coordinates via $(x, y, z) = (r - r_o, r_o[\phi - \Omega_o t - \phi_o], z)$. We assume throughout that the disk is isothermal ($p = c_s^2 \rho$, where c_s is constant), and that the disk orbits in a Keplerian ($1/r$) potential.

In the local model, the momentum equation of ideal MHD becomes

$$\frac{\partial \boldsymbol{v}}{\partial t} + \boldsymbol{v}\cdot\boldsymbol{\nabla}\boldsymbol{v} + c_s^2\frac{\boldsymbol{\nabla}\rho}{\rho} + \frac{\boldsymbol{\nabla}B^2}{8\pi\rho} - \frac{(\boldsymbol{B}\cdot\boldsymbol{\nabla})\boldsymbol{B}}{4\pi\rho} + 2\boldsymbol{\Omega}\times\boldsymbol{v} - 3\Omega^2 x\,\hat{\boldsymbol{x}} = 0. \quad (1)$$

The final two terms in Equation (1) represent the Coriolis and tidal forces in the local frame. Note that our model is unstratified, which means that the vertical gravitational acceleration $-\Omega^2 z$ usually present in Keplerian disks is ignored.

Our model contains no explicit dissipation coefficients. Recent models with explicit scalar dissipation (FP07; Lesur & Longaretti 2007) have shown that the outcome (saturated field strength) depends on the viscosity ν and the resistivity η, and that ZEUS has an effective magnetic Prandtl number $Pr_M \equiv \nu/\eta \sim 4$.

The orbital velocity in the local model is

$$\boldsymbol{v}_{\rm orb} = -\frac{3}{2}\Omega x\,\hat{\boldsymbol{y}}. \quad (2)$$

This velocity, along with a constant density and zero magnetic field, is a steady-state solution to Equation (1). If the computational domain extends to $|x| > (2/3)H = (2/3)c_s/\Omega$, then the orbital speed is supersonic with respect to the grid.

The local model is studied numerically using the "shearing box" boundary conditions (e.g., Hawley et al. 1995). These boundary conditions isolate a rectangular region in the disk. The azimuthal (y) boundary conditions are periodic; the radial (x) boundary conditions are "nearly periodic," i.e., they connect the radial boundaries in a time-dependent way that enforces the mean shear flow. We use periodic boundary conditions in the vertical direction; this is the simplest possible version of the shearing box model.

2.1. Numerical Methods

Most of our models are evolved using ZEUS (Stone & Norman 1992). ZEUS is an operator-split, finite difference scheme on a staggered mesh. It uses artificial viscosity (not an anomalous viscosity!) to capture shocks. For the magnetic field evolution ZEUS uses the Method of Characteristics-Constrained Transport (MOC-CT) scheme, which is designed to accurately evolve Alfvén waves (MOC) and also to preserve the $\boldsymbol{\nabla}\cdot\boldsymbol{B} = 0$ constraint to machine precision (CT).

We have modified ZEUS to include "orbital advection" (Masset 2000; Gammie 2001; Johnson & Gammie 2005) with a magnetic field (Johnson et al. 2008). Advection by the orbital component of the velocity $\boldsymbol{v}_{\rm orb}$ (which may be supersonic with respect to the grid) is done using interpolation. With this modification the time step condition $\Delta t < C\Delta x/(|\delta\boldsymbol{v}| + c_{\rm max})$ ($c_{\rm max} \equiv$ maximum wave speed and $C \equiv$ Courant number) depends only on the perturbed velocity $\delta\boldsymbol{v} = \boldsymbol{v} - \boldsymbol{v}_{\rm orb}$ rather than $\boldsymbol{v}$. So when $|\boldsymbol{v}_{\rm orb}| \gtrsim c_{\rm max}$ (for shearing box models with $v_A^2/c_s^2 \lesssim 1$, when $L \gtrsim H$) the time step can be larger with orbital advection, and computational efficiency is improved.

Orbital advection also improves accuracy. ZEUS, like most Eulerian schemes, has a truncation error that increases as the speed of the fluid increases in the grid frame. In the shearing box without orbital advection the truncation error would then increase monotonically with $|x|$. Orbital advection reduces the amplitude of the truncation error and also makes it more nearly uniform in $|x|$ (Johnson et al. 2008).

Do our results depend on the algorithm used to integrate the MHD equations? To find out, we have also evolved a subset of models using ATHENA, a second-order accurate Godunov scheme that solves the equations of ideal MHD in conservative form. The algorithm couples the dimensionally unsplit corner transport upwind (CTU) method of Colella (1990) with the third-order in space piecewise parabolic method (PPM) of Colella & Woodward (1984), and a constrained transport (CT) algorithm for preserving the $\boldsymbol{\nabla}\cdot\boldsymbol{B} = 0$ constraint. Details of the algorithm and test problems are described in Stone et al. (2008). The specific application of ATHENA to the shearing box (as used in this work) is described in Simon et al. (2009).[5]

2.2. Models with Zero Net Flux

We now consider a set of zero net field shearing box models to introduce our correlation function analysis. We use the same model parameters as FP07 so that these models also serve, by comparison with FP07, as a nonlinear code test.

The models in this section have size $(L_x, L_y, L_z) = (1, \pi, 1)H$. The initial magnetic field is $B_z = B_{z0}\times\sin(2\pi x/H)$, where B_{z0} satisfies $\beta \equiv 8\pi P_0/B_{z0}^2 = 400$. Noise is introduced in the initial velocity field to stimulate the growth of the unstable modes. The models are evolved to $t_f = 600\,\Omega^{-1}$.

We consider four resolutions: $(N_x, N_y, N_z) = N(32, 50, 32)$, where $N = 1, 2, 4, 8$. The last three models correspond to runs std32, std64, and std128 in FP07, respectively. The evolution of $\langle E_B\rangle \equiv \langle B^2/(8\pi\rho_o c_s^2)\rangle$ is shown in Figure 1 ($\langle\rangle \equiv$ volume average). The saturation $\langle E_B\rangle$ decreases as the resolution increases.

The dimensionless shear stress

$$\alpha \equiv \frac{\left\langle \rho v_x \delta v_y - \frac{B_x B_y}{4\pi}\right\rangle}{\langle\rho\rangle c_s^2}. \quad (3)$$

[5] Simon et al. (2009) use $P = (\gamma - 1)\,u$ in contrast to our $P = c_s^2\rho$.

Table 1
Shearing Box Runs with a Zero Net Vertical Field

Model	Resolution	$\overline{\alpha}$	$\lambda_{B,\min}$	$\lambda_{B,\mathrm{maj}}$	$\lambda_{B,z}$	$\theta_{B,\mathrm{tilt}}$	$\lambda_{v,\min}$	$\lambda_{v,\mathrm{maj}}$	$\lambda_{v,z}$	$\theta_{v,\mathrm{tilt}}$	$\lambda_{\rho,\min}$	$\lambda_{\rho,\mathrm{maj}}$	$\lambda_{\rho,z}$	$\theta_{\rho,\mathrm{tilt}}$
$z32$	$32 \times 50 \times 32$	3.8×10^{-3}	0.090	0.62	0.080	11	0.078	0.57	0.13	5.5	0.076	0.82	0.39	8.6
$z64$	$64 \times 100 \times 64$	4.2×10^{-3}	0.059	0.38	0.050	13	0.074	0.45	0.18	7.1	0.056	0.60	0.33	6.6
$z128$	$128 \times 200 \times 128$	2.1×10^{-3}	0.037	0.22	0.032	14	0.053	0.32	0.11	6.7	0.043	0.62	0.33	6.4
$z256$	$256 \times 400 \times 256$	1.1×10^{-3}	0.024	0.17	0.024	14	0.035	0.24	0.10	5.9	0.019	0.34	0.18	5.8

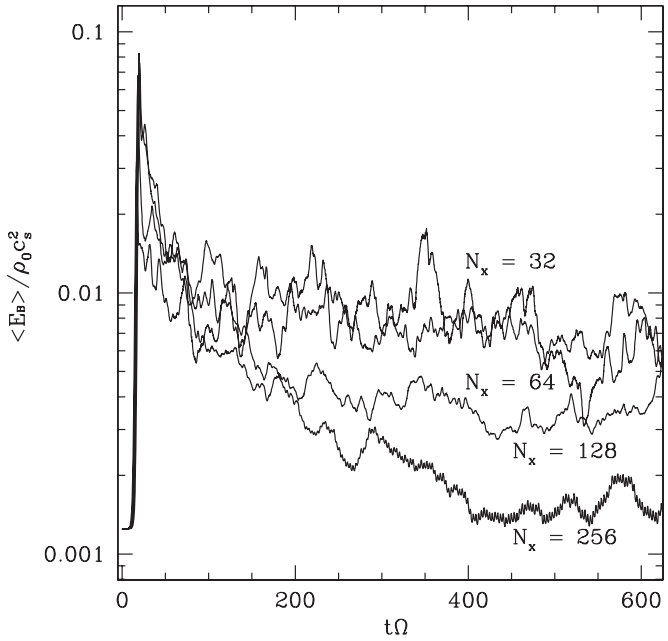

Figure 1. Evolution of magnetic energy in zero net field runs. From top to bottom radial resolution increases from $32/H$, $64/H$, $128/H$ to $256/H$. The saturation level decreases in proportion to the grid scale.

We measured the time average of α, denoted as $\overline{\alpha}$, (from $t\Omega = 250$ to $t\Omega = 600$) for each run, and recorded the results in Table 1.[6] These averages are nearly identical to those obtained by FP07. This consistency enhances confidence in both sets of results.

For $N_x \geqslant 64$

$$\overline{\alpha} \simeq 0.0021 \left(\frac{N_x}{128}\right)^{-1} \tag{4}$$

is a good fit to the numerical results. The magnetic field energy density, α, and the kinetic energy density are almost inversely proportional to N_x, and so, like FP07, we conclude that the zero net field models do not converge.

All shearing box models considered in this paper have $\overline{\alpha} \simeq \overline{\langle E_B \rangle}/2 = 1/(2\overline{\beta})$. This implies a characteristic orientation of the field, since (neglecting the Reynolds stress $\rho v_x v_y \sim 0.25 \times [-B_x B_y]/[4\pi]$) $\overline{\alpha} \approx -\overline{\langle B_x B_y \rangle}/(4\pi \langle \rho \rangle c_s^2) \equiv \overline{\langle B^2 \cos\theta_B \sin\theta_B \rangle}/(4\pi \langle \rho \rangle c_s^2)$, where θ_B is the angle between the field and the y-axis. Then $\overline{\alpha} = \overline{\langle E_B \rangle} 2 \cos\overline{\theta}_B \sin\overline{\theta}_B = \overline{\langle E_B \rangle}/2$. So $\overline{\theta}_B = \pi/12$ (15°) is the characteristic angle between the magnetic field and the y-axis.

[6] The combination of finite run time and fluctuations in $\alpha(t)$ introduces noise into $\overline{\alpha}$. To estimate the noise amplitude we divided the averaging interval into two and compared the two averages. In all the runs with $N_x \geqslant 64$ case they differed from the mean by $\leqslant$10%.

Next, we turn to the structure of the zero net field turbulence. Consider the two-point correlation function for the density fluctuations

$$\xi_\rho \equiv \langle \delta\rho(\boldsymbol{x}) \delta\rho(\boldsymbol{x} + \Delta\boldsymbol{x}) \rangle \tag{5}$$

($\delta\rho \equiv \rho - \langle\rho\rangle$), for the trace of the velocity fluctuation correlation tensor

$$\xi_v = \langle \delta v_i(\boldsymbol{x}) \delta v_i(\boldsymbol{x} + \Delta\boldsymbol{x}) \rangle \tag{6}$$

($\delta v_i \equiv v_i - v_{i,orb} - \langle v_i \rangle$), and there is an implied summation over i and for the trace of the magnetic field correlation tensor

$$\xi_B = \langle \delta B_i(\boldsymbol{x}) \delta B_i(\boldsymbol{x} + \Delta\boldsymbol{x}) \rangle \tag{7}$$

($\delta B_i \equiv B_i - \langle B_i \rangle$). All correlation functions are calculated for fluctuating dynamical variables with zero mean. Figure 2 shows slices of correlation functions through ξ at $z = 0$ for run $z128$. The cores of the correlation functions are ellipsoidal, with three principal axes, and concentrated at $|\Delta\boldsymbol{x}| < H$. The correlations are localized.

We measure four features of the correlation functions: the angle θ_{tilt} between the correlation function major axis and the y-axis, and the correlation lengths along the major, minor, and z-axes (λ_{maj}, $\lambda_{\min}$, λ_z), where the correlation length λ_i is defined[7] by

$$\lambda_i \equiv \frac{1}{\xi(0)} \int_0^\infty \xi(\hat{\boldsymbol{x}}_i l) dl. \tag{8}$$

l is the distance from $\Delta\boldsymbol{x} = 0$ along the principal axis defined by the unit vector $\hat{\boldsymbol{x}}_i$, and $\hat{\boldsymbol{x}}_{\mathrm{maj}} = \hat{\boldsymbol{x}} \sin\theta_{\mathrm{tilt}} - \hat{\boldsymbol{y}} \cos\theta_{\mathrm{tilt}}$, $\hat{\boldsymbol{x}}_{\min} = \hat{\boldsymbol{x}} \cos\theta_{\mathrm{tilt}} + \hat{\boldsymbol{y}} \sin\theta_{\mathrm{tilt}}$, and $\hat{\boldsymbol{x}}_z = \hat{\boldsymbol{z}}$.[8,9] Figure 3 shows ξ_B along each of the principal axes in run $z128$. The dotted lines show $\xi(0)\exp(-l/\lambda_i)$. The correlated regions in the magnetic field are narrow ($\lambda_{\min} \simeq \lambda_z \simeq \lambda_{\mathrm{maj}}/6$) filaments with a trailing spiral orientation.

What do the correlation functions mean? For the magnetic field, there is a characteristic orientation of the field $\overline{\theta}_B$ obtained through our measurement of the shear stress. The major axis of the correlation function is very nearly parallel to this, $\theta_{\mathrm{tilt}} \simeq \overline{\theta}_B$. It is reasonable to view the magnetic field correlation function, then, as tracing out a characteristic, filamentary structure in the magnetic field.

It is worth recalling briefly what we might expect for ξ_v in isotropic, homogeneous turbulence with an outer scale $L_0 = 2\pi/k_0$ and velocity dispersion σ_v. In the inertial range

[7] Other definitions of λ_i are possible, e.g., the half-width at half-maximum (HWHM) of ξ can be used, with an exponential model for ξ, to find λ_i. For example, for ξ_B in run $z128$, the HWHM definition gives (λ_{maj}, $\lambda_{\min}$, λ_z) = $(0.031, 0.15, 0.023)H$ compared to $(0.026, 0.15, 0.022)H$ from our definition. The differences are less than 20%.

[8] In a periodic domain $\int d^3\Delta x_f \xi = 0$ if $\int d^3x f = 0$, but this does not imply that the line integral in Equation (8) vanishes.

[9] The integral in Equation (8) is evaluated by linearly interpolating ξ in the Δx–Δy plane and summing over the interpolated values (trapezoidal rule) along the principal axis. We evaluate the line integral until $\xi(l) = e^{-3}\xi(0)$. The result is insensitive to the upper limit on the integral.

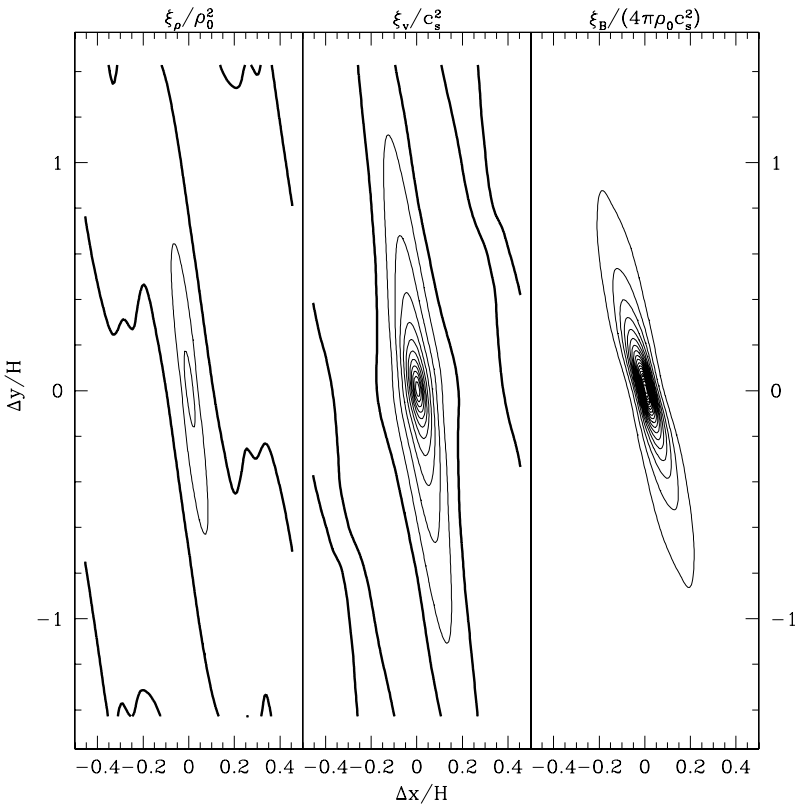

Figure 2. Two-point correlation function for density, velocity field, and magnetic field in Δx–Δy plane in run $z128$. The contours are set linearly from 0 to 0.009 for 20 levels; the heavy line is the 0 contour.

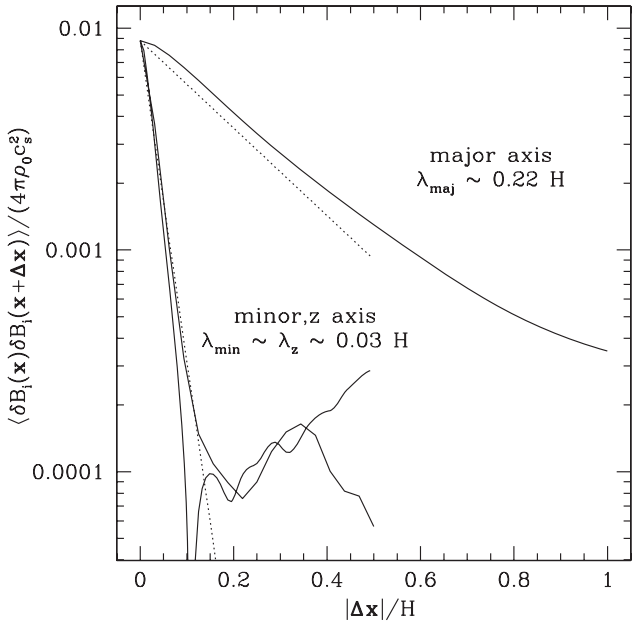

Figure 3. Magnetic field correlation function along the minor, major, and vertical principle axes in run $z128$. Solid lines: cut through the data; dotted lines: a simple model with $\exp(-\lambda_i)$, where λ_i is the measured correlation length along each principle axis. The correlation functions along the minor and z-axes are almost identical.

$v_k^2 \propto k^{-11/3}$, so a reasonable functional form for the power spectrum is

$$v_k^2 = N \left(\frac{\sigma_v^2}{k_0^3}\right) \frac{1}{(1+(k/k_0)^2)^{11/6}}, \tag{9}$$

where N is a nondimensional normalization constant. The corresponding autocorrelation function is

$$\xi_v = \sigma_v^2 \frac{\sqrt{3}\Gamma\left(\frac{2}{3}\right)}{2^{1/3}\pi} (k_0 r)^{1/3} K_{1/3}(k_0 r), \tag{10}$$

where K is the modified Bessel function and $r \equiv |\Delta x|$. For $k_0 r \ll 1$,

$$\xi_v \approx \sigma_v^2 (1 - 0.955\,(k_0 r)^{2/3} + O(r^2)). \tag{11}$$

This is the usual $r^{2/3}$ Kolmogorov dependence at small separation. For $k_0 r \gg 1$,

$$\xi_v \approx \sigma_v^2\ 0.743\ (k_0 r)^{-1/6}\, e^{-k_0 r}, \tag{12}$$

which yields the expected decorrelation for $k_0 r \gg 1$. The correlation length defined in Equation (8) is $0.838/k_0$. Note that the power spectrum does not have zero power as $k \to 0$; rather it asymptotes to $N\sigma_v^2 k_0^{-3}$.

For MHD turbulence in disks, however, the correlation function is not isotropic, and its structure is not anticipated by any predictive theory. In the absence of such a theory it may be useful to have a convenient analytical representation of the numerical results. This can be obtained by stretching Equation (10) along each of the principal axes, that is, by replacing $k_0 r$ by $u \equiv ((\Delta\boldsymbol{x} \cdot \hat{\boldsymbol{x}}_{\rm min}/\lambda_{\rm min})^2 + (\Delta\boldsymbol{x} \cdot \hat{\boldsymbol{x}}_{\rm maj}/\lambda_{\rm maj})^2 + (\Delta\boldsymbol{x} \cdot \hat{\boldsymbol{x}}_z/\lambda_z)^2)^{1/2}$.

Do the correlation lengths converge? We find that the correlation lengths are resolution dependent, with

$$(\lambda_{\rm min}, \lambda_{\rm maj}, \lambda_z) \simeq (0.04, 0.24, 0.03)\, H \left(\frac{N_x}{128}\right)^{-2/3}; \tag{13}$$

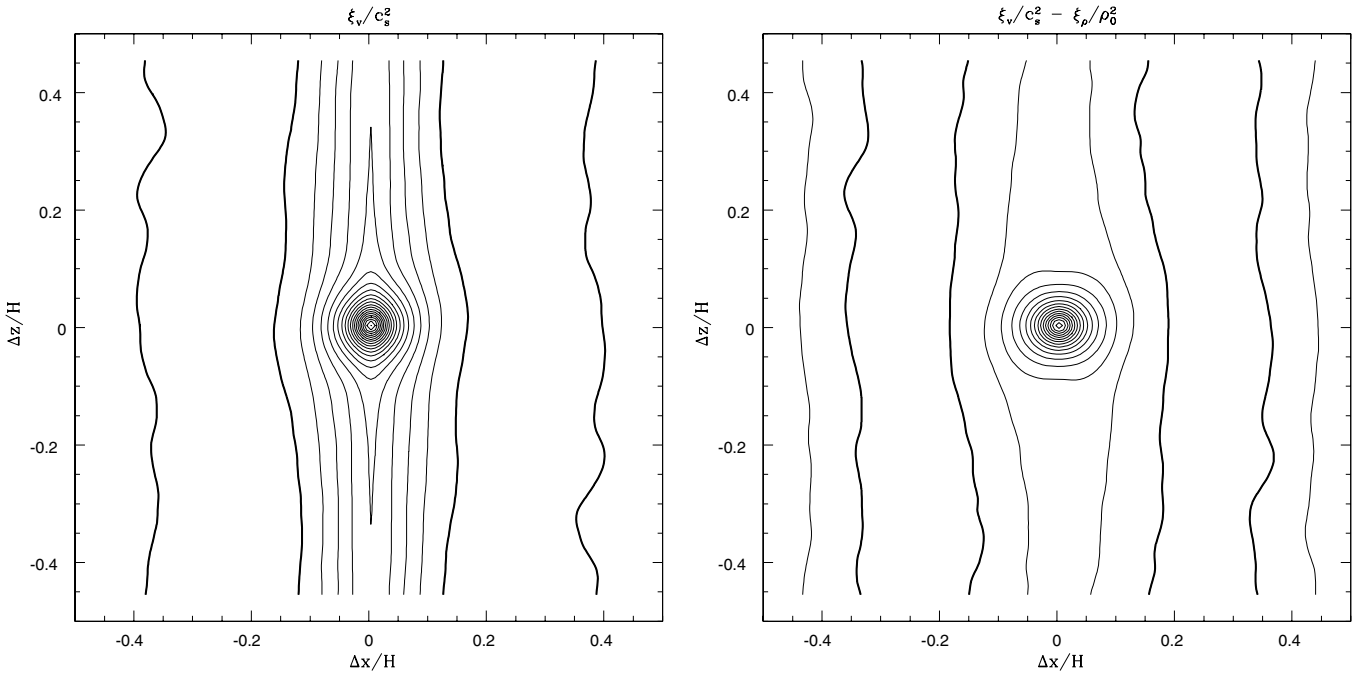

Figure 4. Turbulent velocity correlation function and a differential correlation $\xi_v/c_s^2 - \xi_\rho/\rho_0^2$ in the $\Delta y = 0$ plane for run $z128$. In ξ_v, apart from the compact core at small separations, there is a weak correlation at large scales that is likely due to the sound waves. The contours run linearly from 0 to 0.005 for 20 levels. The heavy line is the 0 contour.

λ_z and $\lambda_{\rm min}$ are at most six zones. The scaling of $\lambda_{\rm min}$ with zone size is clearly not linear, but the 2/3 power-law scaling is just a fit to the data and should not be taken too seriously. The nonlinear scaling does hint at the possibility that, as resolution is increased and $\lambda_{\rm min}$ and λ_z are better resolved, there could be a transition in the outcome.

The major axis for ξ_B lies $\sim 15^\circ$ from the y-axis. For the density and peculiar velocity field the tilt angle is $\sim 7^\circ$. The latter tilt is consistent with the measured Reynolds stress: $\langle \rho v_x v_y \rangle / \langle \rho v^2 \rangle \sim 1/8$, so the average perturbed velocity is tilted at $\sim 7^\circ$ to the y-axis.

Finally, note that there are low-amplitude features in ξ_v and ξ_ρ at scales of a few correlation lengths (see particularly in Figure 4(a)). These features may be due to the excitation of rotationally modified sound waves by MHD turbulence. To test this hypothesis note that, for tightly wrapped ($k_y \ll k_x$), linear sound waves $\delta\rho_k^2/\rho_0^2 \simeq \delta v_k^2/c_s^2$. A field composed of these waves would then have $\xi_\rho/\rho_0^2 = \xi_v/c_s^2$. Taking the differential correlation function $\xi_v/c_s^2 - \xi_\rho/\rho_0^2$ should therefore remove those pieces of ξ_v that are due to sound waves. Figure 4(b) shows $\xi_v/c_s^2 - \xi_\rho/\rho_0^2$ at $\Delta y = 0$. Evidently much of the large-scale power is removed. Figure 5 shows another slice through $\xi_v/c_s^2 - \xi_\rho/\rho_0^2$ at $\Delta z = 0$. Again the large-scale power is removed. This is consistent with the hypothesis that the largest scale features in the correlation functions are acoustic waves.

3. MODELS WITH A NET AZIMUTHAL FIELD

In this section, we study models with $\langle B_y \rangle \neq 0$. These models correspond more closely to what is observed in shearing box models with boundary conditions that allow the net field to evolve, what is seen in global MHD models of disks, and what is observed in galactic disks than the $\langle \boldsymbol{B} \rangle = 0$ models.

3.1. Convergence

To test convergence we use the same size models as the zero net field runs, $(L_x, L_y, L_z) = (1, \pi, 1)H$. $\langle B_y \rangle$ is set so that $\beta = 400$; in the initial conditions all other magnetic field components vanish. The models are evolved to $t = 250\,\Omega^{-1}$. We use five different resolutions: $(N_x, N_y, N_z) = N(32, 50, 32)$, where $N = 1, 2, 4, 6, 8$. In each run we average over the second half of the evolution to measure $\overline{\langle E_B \rangle}$ and $\overline{\alpha}$. We also measure the correlation lengths from ξ_ρ, ξ_v, and ξ_B using an average of the correlation function calculated from eight data dumps in the second half of the run. Parameters and results for these runs are listed in Table 2.

Figure 6 shows $\langle E_B \rangle(t)$ for various resolutions. In our two highest resolution runs, $\overline{\langle E_B \rangle} = 3.7 \times 10^{-2} \rho_0 c_s^2$ for run $y192a$ and $4.1 \times 10^{-2} \rho_0 c_s^2$ for run $y256a$, respectively. A consistent fit is $\overline{\langle E_B \rangle} \simeq 0.03 (N_x/128)^{1/3}$ for $32 < N_x < 256$. The saturation energy increases with resolution. It is unlikely that this trend continues indefinitely. As we will see below, the magnetic field correlation lengths are unresolved at $N_x = 32$ but resolved at $N_x = 256$. This suggests that the increase in $\overline{\langle E_B \rangle}$ is caused by resolution of magnetic structures near the correlation length. If there is little energy in structures much smaller than the correlation length, then $\overline{\langle E_B \rangle}$ should saturate at somewhat higher resolution.

To check the algorithm dependence of the results we ran an identical set of models using ATHENA. The results are listed in Table 2. Both sets of models show a weak upward trend in $\overline{\langle E_B \rangle}$ with resolution. If one corrects for the approximately 2 times higher effective resolution of ATHENA then the ATHENA and ZEUS results are quantitatively consistent with each other.

The correlation lengths for the zero net field runs do not converge. What about the net azimuthal field models? The magnetic field correlation lengths are listed in Table 2 (other correlation lengths are omitted for brevity, but they behave

Table 2
Shearing Box Runs with a Net Azimuthal Field

Model	Algorithm	Resolution	$\overline{\alpha}$	$\overline{\langle E_B \rangle}/\rho_0 c_s^2$	$\lambda_{B,\min}$	$\lambda_{B,\mathrm{maj}}$	$\lambda_{B,z}$	$\theta_{B,\mathrm{tilt}}$	$\lambda_{B,\min}/\Delta x$
*y*32*a*	ZEUS	$32 \times 50 \times 32$	0.0094	0.019	0.10	0.40	0.084	12	3.2
*y*64*a*	ZEUS	$64 \times 100 \times 64$	0.014	0.024	0.066	0.36	0.064	15	4.2
*y*128*a*	ZEUS	$128 \times 200 \times 128$	0.015	0.028	0.053	0.28	0.049	15	6.8
*y*192*a*	ZEUS	$192 \times 300 \times 192$	0.020	0.037	0.055	0.30	0.049	15	11
*y*256*a*	ZEUS	$256 \times 400 \times 256$	0.021	0.041	0.049	0.27	0.045	15	13
*y*32*b*	ATHENA	$32 \times 50 \times 32$	0.018	0.032	0.11	0.63	0.09	15	3.3
*y*64*b*	ATHENA	$64 \times 100 \times 64$	0.015	0.027	0.070	0.38	0.060	16	4.5
*y*128*b*	ATHENA	$128 \times 200 \times 128$	0.018	0.035	0.058	0.33	0.051	16	7.4
*y*192*b*	ATHENA	$192 \times 300 \times 192$	0.025	0.050	0.052	0.30	0.047	17	10
*y*256*b*	ATHENA	$256 \times 400 \times 256$	0.027	0.055	0.053	0.32	0.049	16	14

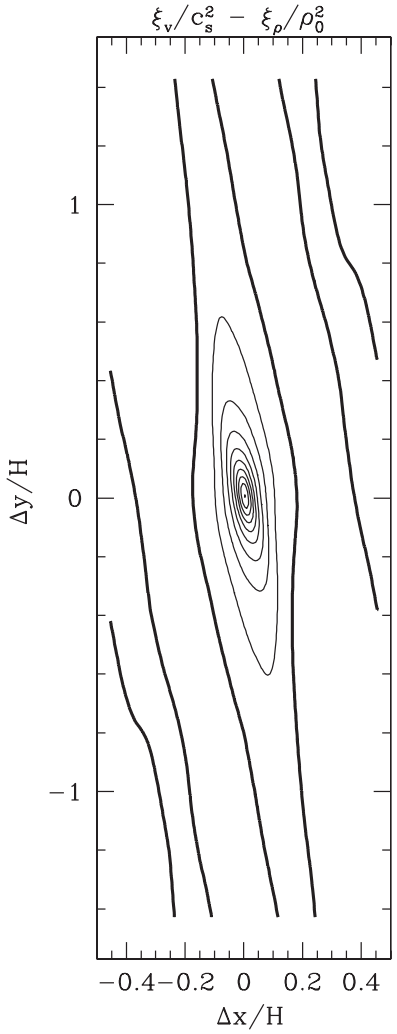

Figure 5. Differential correlation function $\xi_v/c_s^2 - \xi_\rho/\rho_0^2$ in the $\Delta z = 0$ plane in run *z*128. After removing the contribution due to the sound waves, the correlation ellipsoid is more compact and almost identical to that of the magnetic field. The contour levels are set the same as in Figure 2, linearly from 0 to 0.009.

similarly). For $N \geqslant 4$ both ZEUS and ATHENA find

$$(\lambda_{\min}, \lambda_{\mathrm{maj}}, \lambda_z) \simeq (0.05, 0.32, 0.05)\, H. \tag{14}$$

For the $N \geqslant 4$ models $\lambda_{\min} \sim \lambda_z > 8\Delta x$. In the highest resolution ($N = 8$) ATHENA model, $\lambda_{\min}/\Delta x \simeq 14$. The correlation lengths are both converged and resolved.

If MHD turbulence in disks has a forward energy cascade, as do three-dimensional hydrodynamic turbulence and the Goldreich–Sridhar model for strong MHD turbulence in a homogeneous medium, then it is natural to identify the correlation lengths with the outer, or energy injection, scale. Since $\lambda_{\min} \simeq 15$ grid zones at our highest resolution there is no resolved inertial range. We anticipate that future, higher-resolution numerical experiments with a mean azimuthal field will show the development of an inertial range.

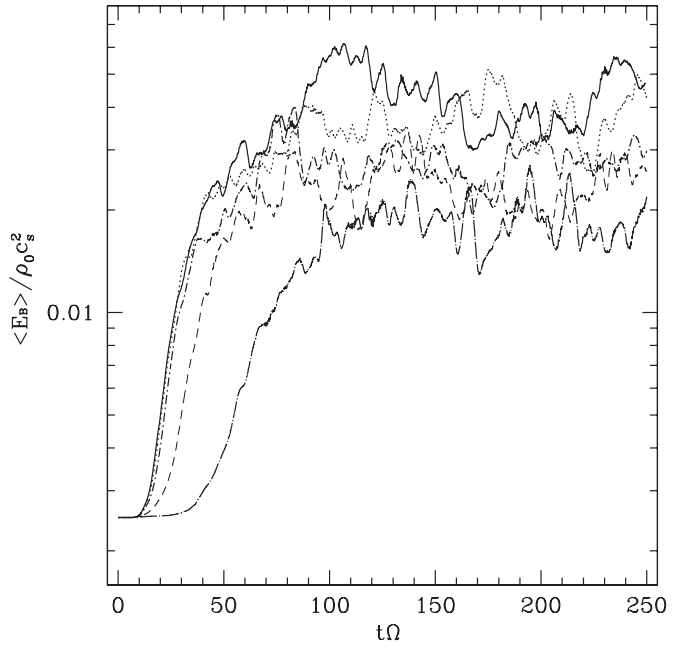

Figure 6. Evolution of the magnetic energy in the net azimuthal field run. From bottom to top the lines are: heavy dot–long dash: $32/H$; gray short dash: $64/H$; heavy dot–short dash: $128/H$; gray dot: $192/H$; heavy solid: $256/H$. The saturation energy increases with resolution.

3.2. Magnetic Energy Evolution

At what scale is magnetic energy generated in MRI-driven turbulence? To investigate this, we have studied the correlation function for each term driving the evolution of the volume-averaged magnetic energy:

$$\dot{E}_B = -\left\langle \boldsymbol{\nabla} \cdot \left(\frac{1}{2} B^2 \boldsymbol{v} \right) \right\rangle - \left\langle \frac{1}{2} B^2 \boldsymbol{\nabla} \cdot \boldsymbol{v} \right\rangle + \langle \boldsymbol{B} \cdot (\boldsymbol{B} \cdot \boldsymbol{\nabla} \boldsymbol{v}) \rangle - D, \tag{15}$$

where D is the volume-averaged numerical dissipation rate. The terms on the right-hand side can be interpreted as describing the effects of advection, compression and expansion, field-line stretching, and numerical dissipation. On average the first term

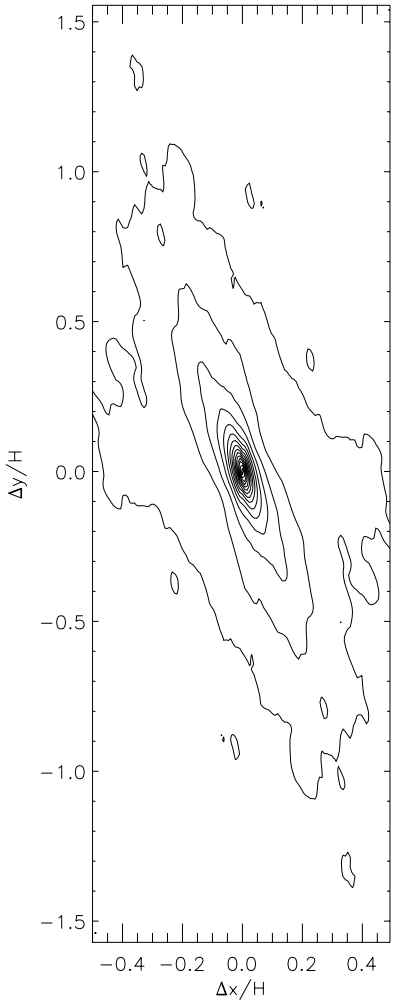

Figure 7. Correlation function in the $\Delta z = 0$ plane for the "field-line stretching" term in the magnetic energy equation. The data are from the $y128b$ `ATHENA` run and the contour levels run logarithmically from $10^{-5.1}$ to $10^{-3.6}$. The generation and dissipation of magnetic energy occurs in a local manner, consistent with the localization of the dynamical variables.

is small (it should vanish exactly for shearing box boundary conditions, but roundoff and truncation error make it nonzero), and the third term dominates the second by a factor of 20 in run $y128b$. In a time- and volume-averaged sense the right-hand side must be zero, so numerical dissipation must approximately balance energy injection by field-line stretching.

Previous studies (FP07; Simon et al. 2009) analyzed a version of this equation in the Fourier domain to study turbulent energy flow as a function of length scale in the shearing box simulations. Both studies found that the magnetic energy is generated on all scales by the background shear. Here, we perform a complementary analysis in the spatial domain.[10]

We have computed the autocorrelation function for the field-line stretching term from run $y128b$ (without subtracting the mean). Figure 7 shows the autocorrelation function at $\Delta z = 0$. From this figure we conclude that: (1) the scale and shape of the correlation function is similar to that of the fundamental variables ($\boldsymbol{B}$, $\boldsymbol{v}$; recall that in $y128$b $(\lambda_{B,\rm min}, \lambda_{B,\rm maj}, \lambda_{B,z}) =$ $(0.058, 0.33, 0.051)H$); (2) energy is injected at scales comparable to the correlation length of the fundamental variables; (3) a superposition of magnetic structures similar to ξ_B that are distributed with uniform probability in space would have a power spectrum that is flat (white noise) at low k. It is plausible that terms in the Fourier-transformed magnetic energy equation would also be flat at low k. This would not imply that energy is injected by dynamically meaningful structures at large scales; it would simply be the consequence of an uncorrelated superposition of small, localized features in the turbulence.

[10] Simon et al. (2009) study the k dependence of analogous terms on the right-hand side of an equation for $|B_k|^2$ (their Equation (19)), which scale like B^2. We directly autocorrelate the terms on the right-hand side of Equation (15), and this scales like B^4.

Table 3
Shearing Box Runs with a Net Azimuthal Field: Effect of the Box Size

Model	Size	$\overline{\langle E_B \rangle}/\rho_0 c_s^2$	$\frac{\lambda_{B,\rm maj}}{H}$
$y64$	$(1, \pi, 1)H$	0.024	0.36
$y64.x2$	$(2, \pi, 1)H$	0.028	0.49
$y64.y2$	$(1, 2\pi, 1)H$	0.035	0.45
$y64.x2y2$	$(2, 2\pi, 1)H$	0.038	0.49
$y64.x4y4$	$(4, 4\pi, 1)H$	0.038	0.57

3.3. Box Size

Does the saturation energy or correlation length depend on the size of the computational domain (box size)? To investigate, we fix the physical resolution at 64 zones/H and vary the model size: $(L_x, L_y, L_z) = (1, \pi, 1)H, (2, \pi, 1)H, (1, 2\pi, 1)H$, $(2, 2\pi, 1)H$, and $(4, 4\pi, 1)H$. The model parameters and outcomes are listed in Table 3.

Evidently, there is a weak dependence of $\overline{\langle E_B \rangle}$ on box size; it increases from $0.024\rho_0 c_s^2$ for the smallest run to $0.038\rho_0 c_s^2$ for the largest run. The magnetic field correlation lengths also increase with box size, with $\lambda_{\rm maj} = 0.36H$ for the smallest box (so $L_y/(2\lambda_{\rm maj}) = 4.4$) to $\lambda_{\rm maj} = 0.57H$ for the largest box (so $L_y/(2\lambda_{\rm maj}) = 11$). This upward trend in correlation length is probably real, but it is sufficiently small that it is difficult to separate from noise in the correlation length measurements.

The correlation functions ξ_ρ and ξ_v, unlike ξ_B, have low amplitude tails extending out to the box size. This can be seen in Figure 8, which shows ξ_ρ and ξ_B for run $y64.x4y4$. The tails are likely due to sound waves, and their absence in the differential correlation function $\xi_v/c_s^2 - \xi_\rho/\rho_0^2$, shown in the middle panel of Figure 8, is consistent with this.

3.4. Field Strength

We now compare two models that differ only in their initial field strength. Both have a size $L_x, L_y, L_z = (1, 2\pi, 1)H$ with resolution $N_x, N_y, N_z = 64, 200, 64$. One model has the same initial field strength as our other models, $\beta_0 = 400$, while the other one starts with a stronger field, $\beta_0 = 100$.

We found that the saturated magnetic energy for the $\beta_0 = 400$ run is $\overline{\langle E_B \rangle} = 0.035\rho_0 c_s^2$. For the $\beta_0 = 100$ run $\overline{\langle E_B \rangle} = 0.079\rho_0 c_s^2$, slightly more than twice the saturation level of the higher β_0 run. Resolution may be playing a role here: the $\beta_0 = 100$ run has twice the resolution per most unstable MRI wavelength, and we know that the saturation level depends on resolution when the field strength is constant.

Our results are consistent with the linear relation between $\overline{\langle E_B \rangle}$ and initial field strength for $\langle B_y \rangle \neq 0$ models reported in Hawley et al. (1995) (hereafter HGB95; although it may also be consistent with a wide range of exponents for this relation). Our results are inconsistent with HGB95's claim that $\overline{\langle E_B \rangle} \propto L_y$, at

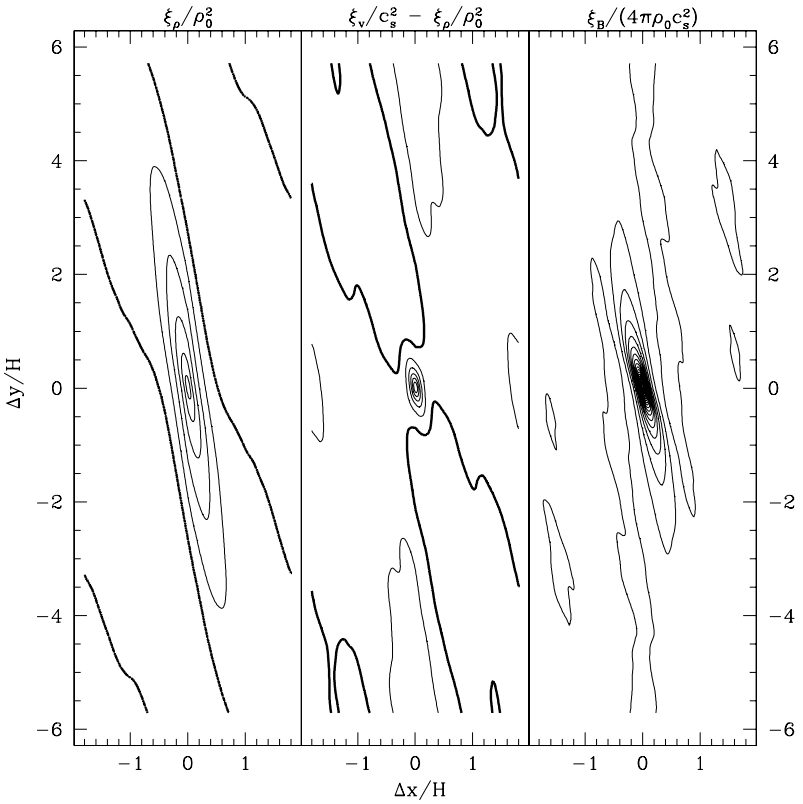

Figure 8. Density correlation function, a differential correlation $\xi_v/c_s^2 - \xi_\rho/\rho_0^2$, and the magnetic correlation function in the $\Delta z = 0$ plane for run $y64.x4y4$. The contours are set linearly from −0.007 to 0.08 for 20 levels. The heavy line is the 0 contour.

least if the box size is $\gg \lambda_{\rm maj}$ (the good agreement found for HGB95's predictor may be a coincidence).

At the level we can determine from two data points, our results are consistent with $\overline{\langle E_B \rangle} \propto \rho_0 c_s V_{A,y0}$, where $V_{A,y0}$ is the initial azimuthal Alfvén speed (i.e., here scale height c_s/Ω replaces L_y in HGB95; there are no other length scales in the problem). This is interesting: it implies that α depends on the gas pressure, a result first reported by Sano et al. (2004) and thus compressibility plays a role in the saturation of the MRI!

Our results suggest that $\overline{\langle E_B \rangle}$ should scale differently in compressible and incompressible models. In the incompressible models the only length scale available is the size of the box, so in incompressible models we must have $\overline{\langle E_B \rangle} \sim \rho_0 (L\Omega)^a V_{A,y0}^b$, where L is some combination of L_x, L_y, and L_z, and the exponents a and b are not determined.

The correlation lengths for the magnetic field in the two runs are $(\lambda_{\rm min}, \lambda_{\rm maj}, \lambda_z) \simeq (0.08, 0.45, 0.08)H$ for the $\beta_0 = 400$ run and $(\lambda_{\rm min}, \lambda_{\rm maj}, \lambda_z) \simeq (0.11, 0.58, 0.10)H$ for the $\beta_0 = 100$ run. To sum up, the correlation length increases weakly as the initial field strength and the box size increases. It is not consistent with the scaling $\sim B_{y,0}/(\rho_0\Omega)$ one would expect if the correlation length scaled with the most unstable wavelength of the background field, and it is not consistent with the scaling $\sim \langle B_y^2 \rangle^{1/2}/(\rho_0\Omega) \sim B_{y,0}^{1/2}$ one would expect if the correlation length is related to a characteristic MRI length scale for the (larger) fluctuating field.

4. SUMMARY

We have investigated the locality of MHD turbulence in an unstratified, Keplerian shearing box model using the two-point autocorrelation function.

We first considered models with zero net vertical field and the same parameters as FP07. Our slightly different orbital advection algorithm reproduces earlier results on the relation between the saturation level and resolution: zero net field models do not converge.

Consistent with this, we also find that as resolution increases the correlation lengths for the velocity, density, and magnetic field decrease. A fit to the results yields the following scaling for the magnetic field correlation lengths,

$$(\lambda_{\rm min}, \lambda_{\rm maj}, \lambda_z) \simeq (0.04, 0.24, 0.03) \left(\frac{N_x}{128}\right)^{-2/3} H, \qquad (16)$$

i.e., the correlation length decreases as the resolution increases.

We then studied a set of models with net toroidal field and initial $\beta = 400$. These models are not completely converged in the sense that they show a trend of increasing $\overline{\alpha}$ with resolution. They are converged in that the correlation lengths are well resolved and constant near the highest resolution:

$$(\lambda_{\rm min}, \lambda_{\rm maj}, \lambda_z) \simeq (0.05, 0.32, 0.05)H. \qquad (17)$$

But because λ_z and λ_{min} are only just resolved (they are each at most 14 grid cells), we do not see an inertial range. We expect that future higher-resolution models will show the development of an inertial range.

We further examined the correlation function for the dominant (nonnumerical) field-line stretching term in the magnetic energy evolution equation. The correlation lengths are small compared to H, consistent with the correlation lengths of the dynamical variables. Evidently, energy is injected at scales comparable to or smaller than the correlation length.

We also explored the influence of the box size on the outcome in the net toroidal field models. We found a weak dependence on the box size but only for $L_x \sim H$. This suggests that in shearing box simulations the size of the box should be chosen to be at least a few scale heights so that the correlation lengths are not "squeezed" by the boundary conditions. We also varied the initial field strength, and consistent with earlier reports found that the saturation level ($\overline{\alpha}$ or $\overline{\langle E_B \rangle}$) scales linearly with the initial field strength. Correlation lengths also increase as the field strength increases, but not linearly.

So is disk turbulence really localized? Our answer is mixed. On the one hand, our net toroidal field models have almost all the correlation amplitudes contained within a region a few scale heights on a side and in this sense the turbulence is indeed local. On the other hand, we do see signs of radiation of compressive waves by the turbulence in the two-point correlation function. These signs are most impressively visible in Figure 4(a), which shows vertically extended tails on the density autocorrelation function in the $\Delta y = 0$ plane, and in Figure 8, which shows azimuthally extended tails on the density autocorrelation function in the $\Delta z = 0$ plane. These tails are matched by similar tails on the velocity autocorrelation function, consistent with our hypothesis that they are due to the excitation of rotationally modified sound waves.

The influence of compressive waves excited by MHD turbulence on disk evolution cannot, in the end, be assessed with the experiments and analysis in this paper. The key measurement needed is the radial damping length of compressive waves due to absorption and scattering of waves by turbulent eddies. This would be most easily measured in a separate experiment that studies the response of MHD turbulence to an imposed sound wave. Even this measurement would be incomplete because it neglects additional damping related to stratification (Lin et al. 1990; Lubow & Ogilvie 1998), but it would provide an upper limit on the damping length.

We are studying the locality of MHD turbulence in a highly idealized situation in which stratification and other aspects of the larger disk—such as the process that generates the imposed azimuthal magnetic field, perhaps a global dynamo—are absent. Our unstratified model is insensitive to some effects that could lead to the development of global ($\lambda \sim R$) or mesoscale ($R \gg \lambda \gg H$) structures. Convection and rotation might reasonably be expected to lead to dynamo activity manifesting itself as large-scale structures in the magnetic field. Disk atmospheres might also develop large-scale, coronal structures that delocalize disk evolution by transmitting angular momentum and energy (Uzdensky & Goodman 2008).

Finite integration time and limited accuracy is also a concern. It is possible that large-scale structures emerge only over hundreds of rotation periods. If the disk is subject to a "viscous instability" of the sort mentioned in the introduction then the timescale for the growth of a feature on scale λ would be $(\alpha\Omega)^{-1}(\lambda/H)^2$; this timescale could be hundreds of rotation periods for the modest αs seen in our models if the instability is damped for $\lambda <$ few $\times H$. Accurate, long duration, and expensive integrations will be required in future searches for viscous instability.

This work was supported by the National Science Foundation under grants AST 00-93091, PHY 02-05155, and AST 07-09246, and a Sony Faculty Fellowship, a University Scholar appointment, and a Richard and Margaret Romano Professorial Scholarship to C.F.G. Portions of this work were completed while C.F.G. was a member at the Institute for Advanced Study (2006–2007). The authors are grateful to Shane Davis, Peter Goldreich, Stu Shapiro, Fred Lamb, Friedrich Meyer, and John Hawley for discussions.

REFERENCES

Balbus, S. A., & Hawley, J. F. 1991, ApJ, 376, 214
Balbus, S. A., & Hawley, J. F. 1998, Rev. Mod. Phys., 70, 1
Beck, R. 2007, EAS Publ. Ser., 23, 19
Beckwith, K., Hawley, J. F., & Krolik, J. H. 2008, ApJ, 678, 1180
Belloni, T., Mendez, M., King, A. R., van der Klis, M., & van Paradijs, J. 1997, ApJ, 479, 145
Brandenburg, A., Nordlund, A., Stein, R., & Torkelsson, U. 1995, ApJ, 446, 741
Colella, P. 1990, J. Comput. Phys., 87, 171
Colella, P., & Woodward, P. R. 1984, J. Comput. Phys., 54, 174
Fromang, S., & Papaloizou, J. 2007, A&A, 476, 1113 (FP07)
Gammie, C. F. 2001, ApJ, 553, 174
Hawley, J. F., Gammie, C. F., & Balbus, S. A. 1995, ApJ, 440, 742 (HGB95)
Hirose, S., Krolik, J., De Villiers, J.-P., & Hawley, J. 2004, ApJ, 606, 1083
Johnson, B. M., & Gammie, C. F. 2005, ApJ, 635, 149
Johnson, B. M., Guan, X., & Gammie, C. F. 2008, ApJS, 177, 373
Lasota, J. P. 2001, New Astron. Rev., 45, 449
Lesur, G., & Longareti, P. Y. 2007, A&A, 378, 1471
Lin, D. N. C., Papaloizou, J. C. B., & Savonije, G. J. 1990, ApJ, 364, 326
Lubow, S. H., & Ogilvie, G. I. 1998, ApJ, 504, 983
Lynden Bell, D., & Pringle, J. E. 1974, MNRAS, 235, 269
Masset, F. 2000, A&AS, 141, 165
McKinney, J. C., & Narayan, R. 2007, MNRAS, 375, 513
Miller, K. A., & Stone, J. M. 2000, ApJ, 534, 398
Piran, T. 1978, ApJ, 221, 652
Sano, T., Inutsuka, S., Turner, N. J., & Stone, J. M. 2004, ApJ, 605, 321
Shakura, N. I., & Sunyaev, R. A. 1973, A&A, 24, 337
Simon, J. B., Hawley, J. F., & Beckwith, K. 2009, ApJ, 690, 974
Spruit, H. C., & Uzdensky, D. A. 2005, ApJ, 629, 960
Stone, J. M., Gardiner, T. A., Teuben, P., Hawley, J. F., & Simon, J. B. 2008, ApJS, 178, 137
Stone, J. M., & Norman, M. L. 1992, ApJS, 80, 753
Uzdensky, D. A., & Goodman, J. 2008, ApJ, 682, 608
van Ballegooijen, A. A. 1989, in Proc. European Physical Society Study Conf. 156, Accretion Disks and Magnetic Fields in Astrophysics, ed. G. Belvedere (Dordrecht: Kluwer), 99